A central amygdala-globus pallidus circuit conveys unconditioned stimulus information and controls fear learning

Jacqueline Giovanniello[1,2], Kai Yu[2 *], Alessandro Furlan[2 *], Gregory Thomas Nachtrab[3], Radhashree Sharma[2], Xiaoke Chen[3], Bo Li[1,2 #]

1. Watson School of Biological Sciences, Cold Spring Harbor Laboratory, Cold Spring Harbor, NY 11724, USA
2. Cold Spring Harbor Laboratory, Cold Spring Harbor, NY 11724, USA
3. Department of Biology, Stanford University, CA 94305, USA

* These authors contributed equally

Correspondence: bli@cshl.edu (B.L.)

Abstract

The central amygdala (CeA) is critically involved in a range of adaptive behaviors. In particular, the somatostatin-expressing (Sst^+) neurons in the CeA are essential for classic fear conditioning. These neurons send long-range projections to several extra-amygdala targets, but the functions of these projections remain elusive. Here, we found in mice that a subset of Sst^+ CeA neurons send projections to the globus pallidus external segment (GPe), and constitute essentially the entire GPe-projecting CeA population. Notably, chronic inhibition of GPe-projecting CeA neurons completely blocks auditory fear conditioning. These neurons are selectively excited by the unconditioned stimulus (US) during fear conditioning, and transient inactivation or activation of these neurons during US presentation impairs or promotes, respectively, fear learning. Our results suggest that a major function of Sst^+ CeA neurons is to represent and convey US information through the CeA-GPe circuit, thereby instructing learning in fear conditioning.

Introduction

The central amygdala (CeA) plays important roles in learning and executing adaptive behaviors. In particular, its function in the acquisition and expression of defensive behaviors has received arguably the most intensive study (Duvarci and Pare, 2014; Herry and Johansen, 2014; Janak and Tye, 2015). For example, transient pharmacological inactivation of the CeA (Goosens and Maren, 2003; Wilensky et al., 2006), or specific inactivation of the lateral division of the CeA (CeL) (Ciocchi et al., 2010), during Pavlovian fear conditioning blocks the formation of fear memories. Moreover, *in vivo* single unit recording demonstrates that fear conditioning causes increased spiking in one CeA population (the "ON" neurons) and decreased spiking in another

(the "OFF" neurons) in response to cues predicting shocks. Such learning-induced changes in the responsiveness of CeA neurons to CS presentations may facilitate the expression of learned defensive responses, including conditioned freezing behavior (Ciocchi et al., 2010; Duvarci et al., 2011; Haubensak et al., 2010). These findings have led to the notion that the CeA, including the CeL, is essential for the formation of aversive memories.

The CeA is a striatal-like structure that contains medium spiny neurons mainly derived from the lateral ganglionic eminence during development (Cassell et al., 1999; Garcia-Lopez et al., 2008; Swanson and Petrovich, 1998; Waraczynski, 2016). These neurons show considerable heterogeneity (Fadok et al., 2018; Li, 2019), which is partly revealed by the different genetic or neurochemical markers that these neurons express. Two of these markers, somatostatin (Sst) (Cassell and Gray, 1989) and protein kinase C-δ (PKC-δ) (Haubensak et al., 2010), label two major populations that are largely nonoverlapping and together constitute about 90% of all neurons in the CeL (Haubensak et al., 2010; Li, 2019; Li et al., 2013).

Recent studies have shown that the excitatory synaptic transmission onto Sst-expressing (Sst^+) CeL neurons is potentiated, whereas that onto Sst-negative (Sst^-) CeL neurons (which are mainly PKC-δ^+ neurons) is weakened by fear conditioning (Ahrens et al., 2018; Hartley et al., 2019; Li et al., 2013; Penzo et al., 2014; Penzo et al., 2015). Consistently, *in vivo* fiber photometry (Yu et al., 2016) or single unit recording (Fadok et al., 2017) studies demonstrate that Sst^+ CeL neurons show increased excitatory responses to shock-predicting cues following fear conditioning, and the responses correlate with freezing behavior (Fadok et al., 2017). Moreover, inhibition of Sst^+

CeL neurons during fear conditioning using chemogenetic (Li et al., 2013; Penzo et al., 2015), optogenetic (Li et al., 2013) or molecular (Yu et al., 2017) methods, which can abolish the fear conditioning-induced potentiation of excitatory synapses onto these neurons (Li et al., 2013; Penzo et al., 2015), impairs the formation of fear memories. These studies provide compelling evidence that Sst^+ CeL neurons constitute an important element of the circuitry underlying fear conditioning.

In light of previous findings about the organization of CeA circuit (Duvarci and Pare, 2014; Fadok et al., 2018; Herry and Johansen, 2014; Li, 2019), Sst^+ CeL neurons can potentially influence fear conditioning via their inhibitory interactions with other neurons locally within the CeL and the resulting disinhibition of the CeM (Ciocchi et al., 2010; Li et al., 2013), a structure that has been shown to control the expression of freezing behavior during fear conditioning through interactions with the midbrain periaqueductal gray (PAG) (Davis, 2000; Duvarci et al., 2011; Fadok et al., 2017; Krettek and Price, 1978; LeDoux et al., 1988; Tovote et al., 2016; Veening et al., 1984). Alternatively, or in addition, as Sst^+ CeL neurons also project to many areas outside of the CeA (Ahrens et al., 2018; Fadok et al., 2018; Li, 2019; Penzo et al., 2014; Steinberg et al., 2020; Ye and Veinante, 2019; Yu et al., 2017; Zhou et al., 2018), these neurons may influence fear conditioning through their long-range projections to extra-CeA structures.

Here, we discovered that a subset of Sst^+ CeA neurons send projections to the globus pallidus external segment (GPe), a basal ganglia structure that is best known for its role in motor control (Kita, 2007; Wallace et al., 2017) but has also been implicated in regulating emotions or affects,

including fear or threat, in both humans and animals (Baumann et al., 1999; Binelli et al., 2014; Blanchard et al., 1981; Critchley et al., 2001; Hattingh et al., 2012; Hernadi et al., 1997; Ipser et al., 2013; Kertes et al., 2009; Murphy et al., 2003; Shucard et al., 2012; Sztainberg et al., 2011; Talalaenko et al., 2006). Furthermore, through *in vivo* fiber photometry and molecular and optogenetic manipulations, we revealed that this previously unknown $Sst^{CeA\text{-}GPe}$ circuit has a critical role in representing the aversive stimulus and instructing learning during fear conditioning.

Results

CeA to GPe projections originate from Sst^{+} neurons

It has been reported that the CeA sends projections to the GPe (Shinonaga et al., 1992). We started to verify this result by using a retrograde tracing approach (Figure 1A). We injected a retrograde adeno-associated virus (AAVrg) encoding the Cre recombinase (AAVrg-Cre) into the GPe of *LSL-H2B-GFP* reporter mice (He et al., 2012), which express the fluorescent protein H2B-GFP (nuclear GFP) in a Cre-dependent manner. This approach led to the labeling of many neurons in the CeA (Figure 1B), confirming the existence of the CeA-GPe pathway.

To determine the main composition of CeA neurons projecting to the GPe, we injected the GPe in wild-type mice with the retrograde tracer cholera toxin subunit B (CTB) conjugated with Alexa Fluor™ 555 (CTB-555) (Figure 1C). We subsequently assessed the expression of *Sst* and *Prkcd* (which encodes PKC-δ) in the CTB-labeled GPe-projecting CeA neurons using single molecule fluorescent *in situ* hybridization (smFISH) (Figure 1D). This approach revealed that the

vast majority of GPe-projecting CeA neurons expresses *Sst* (93±3%; mean±s.e.m.), whereas only a small portion of these neurons expresses either *Prkcd* (6±1%) alone, both *Sst* and *Prkcd* (3±1%), or neither of these molecules (5±3%) (Figure 1E). Similarly, retrograde tracing with CTB in *Sst-IRES-Cre;Ai14* mice, in which Sst^+ cells are labeled with the fluorescent protein tdTomato (Madisen et al., 2010), showed that almost all the GPe-projecting CeA neurons are Sst^+ (92±2%; n = 4 mice) (Figure 1F, G).

In a complimentary experiment, we visualized the CeA-GPe pathway using an anterograde tracing approach. An adeno-associated virus (AAV) expressing the fluorescent protein mCherry in a Cre-dependent manner was injected into the CeA of *Sst-IRES-Cre* mice to label Sst^+ CeA neurons (Figure 1H). Four to five weeks later, we examined the brain sections from these mice for axon fibers originating from the infected Sst^+ CeA neurons. Dense fibers were identified in the dorsal part of the GPe (Figure 1I). Together, these results demonstrate that projections from the CeA to the GPe originate predominantly from Sst^+ neurons (hereafter referred to as $Sst^{CeA\text{-}GPe}$ neurons).

Next, we examined the functional connectivity between $Sst^{CeA\text{-}GPe}$ neurons and the GPe (Figure S1). We introduced the light-gated cation channel channelrhodopsin (ChR2) selectively into Sst^+ CeA neurons of *Sst-IRES-Cre* mice, and used these mice to prepare acute brain slices containing the GPe, in which we recorded synaptic responses in neurons in response to light-simulation of the axons originating from $Sst^{CeA\text{-}GPe}$ neurons (Figure S1A, B). About half of the neurons (5 out of 12) recorded in the GPe showed fast light-evoked inhibitory synaptic responses (Figure S1C),

indicating that $Sst^{CeA\text{-}GPe}$ neurons provide monosynaptic inhibition onto a subset of GPe neurons.

It is known that Sst^{+} CeA neurons send projections to many downstream structures (Ahrens et al., 2018; Fadok et al., 2017; Li, 2019; Penzo et al., 2014; Ye and Veinante, 2019; Yu et al., 2017; Zhou et al., 2018). Therefore, we examined whether $Sst^{CeA\text{-}GPe}$ neurons send collateral projections to another major target of the CeA, the bed nucleus of the stria terminalis (BNST), because our recent study shows that BNST-projecting CeA neurons are also predominantly Sst^{+}, and these neurons play a critical role in anxiety-related behaviors (Ahrens et al., 2018). To this end, we injected both the GPe and the BNST in the same mice with CTB conjugated with different fluorophores, such that GPe-projecting neurons and BNST-projecting neurons in the CeA were labeled with distinct colors (Figure S2A-C). Notably, we found almost no doubly labeled neurons in the CeA in these mice (<1%; Figure S2D), indicating that $Sst^{CeA\text{-}GPe}$ neurons and $Sst^{CeA\text{-}BNST}$ neurons are distinct populations.

$Sst^{CeA\text{-}GPe}$ neurons are necessary for fear learning

As both Sst^{+} CeA neurons (Fadok et al., 2018; Li, 2019) and the GPe (Blanchard et al., 1981; Hattingh et al., 2012; Ipser et al., 2013; Kertes et al., 2009; Murphy et al., 2003; Sztainberg et al., 2011; Talalaenko et al., 2006) have been implicated in processing negative affects including fear, we set out to examine the role of $Sst^{CeA\text{-}GPe}$ neurons in Pavlovian fear conditioning. To determine whether $Sst^{CeA\text{-}GPe}$ neurons are necessary for fear conditioning, we selectively blocked neurotransmitter release from these neurons with the tetanus toxin light chain (TeLC) (Murray et al., 2011). To this end, we used an intersectional viral strategy in wild-type mice, in which we

147 bilaterally injected the GPe with the AAVrg-Cre and the CeA with an AAV expressing TeLC-
148 GFP, or GFP (as the control), in a Cre-dependent manner (Figure 2A, B). Four weeks following
149 viral injection, both the TeLC group and the GFP control group were trained in an auditory fear
150 conditioning paradigm whereby one sound (the conditioned stimulus, or CS^+) was paired with a
151 foot shock (the unconditioned stimulus, or US), and another sound (the neutral sound, or CS^-)
152 was not paired with any outcome (Figure 2C; Figure S3A; Methods).

153

154 Remarkably, blocking transmitter release from $Sst^{CeA\text{-}GPe}$ neurons with TeLC completely
155 abolished the conditioned freezing induced by CS^+ during a memory retrieval test 24 hours after
156 the conditioning (Figure 2C). Furthermore, this manipulation also reduced the responses of the
157 mice to foot-shocks, as indicated by a reduction in the peak velocity of shock-induced
158 movements (Figure 2D). These results indicate that $Sst^{CeA\text{-}GPe}$ neurons are indispensable for fear
159 conditioning, and suggest that these neurons have a role in processing information about the
160 aversive US.

161

162 **$Sst^{CeA\text{-}GPe}$ neurons represent the unconditioned stimulus during fear conditioning**

163 To further understand the *in vivo* function of $Sst^{CeA\text{-}GPe}$ neurons, we recorded the activities of
164 these neurons in behaving mice. For this purpose, we introduced the genetically encoded calcium
165 indicator GCaMP6 (Chen et al., 2013) into these neurons using the above described
166 intersectional viral strategy, in which we injected the AAVrg-Cre unilaterally into the GPe
167 (Figure 1C, D; Figure 2A), and an AAV expressing GCaMP6 in a Cre-dependent manner into
168 the ipsilateral CeA (Figure 3A, B) in wild-type mice. These mice were then implanted with

optical fibers above the infected area in the CeA (Figure 3A, B; Figure S4). Four weeks after the surgery, we trained the mice in auditory fear conditioning as described above (Figure 2C), and verified that these mice showed discriminative learning as indicated by higher freezing levels to CS^+ than to CS^- during the memory retrieval test (Figure 3C).

We recorded bulk GCaMP6 signals from the infected $Sst^{CeA\text{-}GPe}$ neurons in these animals with fiber photometry (Yu et al., 2016) throughout fear conditioning (Figure 3A-D; Figure S4). In this experiment, we simultaneously recorded both the calcium-dependent signals and the isosbestic signals from the GCaMP6 (Figure 3D), with the latter serving to monitor potential motion artifacts (Kim et al., 2016). Notably, we found that $Sst^{CeA\text{-}GPe}$ neurons showed potent excitatory response to US (shock) presentations during conditioning, but little response to CS^+ (or CS^-) presentations during either conditioning or the memory retrieval test (Figure 3D, E). This result is in sharp contrast with those from Sst^+ CeA neurons with unknown projection targets, which show robust excitatory responses to CS after fear conditioning as assessed by *in vivo* single unit recording (Fadok et al., 2017) or fiber photometry (Yu et al., 2016). Further examination revealed that the responses of $Sst^{CeA\text{-}GPe}$ neurons were significantly higher to stronger shocks than to weaker ones (Figure S5), indicating that the responses represent shock intensity. These results point to the possibility that $Sst^{CeA\text{-}GPe}$ neurons play an important role in processing US information thereby instructing learning in fear conditioning.

$Sst^{CeA\text{-}GPe}$ neuron activity during US presentation is required for learning

To determine whether the excitatory response of $Sst^{CeA\text{-}GPe}$ neurons evoked by US during fear

conditioning is required for learning, we sought to transiently inhibit these neurons only during the presentation of the US. To achieve this goal, we introduced the light sensitive *Guillardia theta* anion-conducting channelrhodopsin 1 (GtACR1) (Govorunova et al., 2015; Mahn et al., 2018) selectively into $Sst^{CeA\text{-}GPe}$ neurons using the intersectional viral strategy described above (Figure 1C, D; Figure 2A, B; Figure 3A, B). Specifically, we injected the AAVrg-Cre bilaterally into the GPe and an AAV expressing GtACR1, or GFP, in a Cre-dependent manner bilaterally into the CeA, followed by implanting optical fibers above the infected areas (Figure 4A; Figure S6).

Four weeks following viral injection, both the GtACR1 group and the GFP group (which served as the control) were trained in the auditory fear conditioning paradigm (Figure 4B; Figure S3B). During conditioning, square pulses of blue light, covering the duration of the three US presentations, were delivered to the CeA through the implanted optical fibers (Figure 4B). Notably, we found that this manipulation caused a decrease in CS^+-induced conditioned freezing behavior in the GtACR1 mice compared with the GFP mice in the retrieval test 24 hours after fear conditioning (Figure 4B). As a result, the ability to discriminate between CS^+ and CS^-, quantified as a discrimination index (Methods), was also reduced in the GtACR1 mice (Figure 4C). We next tested these mice in a real-time place preference or aversion (RTPP or RTPA, respectively) task, in which the photo-inhibition was contingent on entering one side of a chamber containing two compartments (Figure 4D). The two groups of animals behaved similarly in this task (Figure 4E), showing no preference or aversion to either side of the chamber. This observation suggests that photo-inhibition of $Sst^{CeA\text{-}GPe}$ neurons is not inherently aversive or rewarding. These results indicate that the activities of $Sst^{CeA\text{-}GPe}$ neurons during US

presentation are required for memory formation in fear conditioning.

Activation of $Sst^{CeA\text{-}GPe}$ neurons during US presentation promotes fear learning

Given that inhibition of $Sst^{CeA\text{-}GPe}$ neurons specifically during US presentation impaired learning (Figure 4), it follows that the opposite manipulation, i.e., activation of these neurons specifically during US presentation, might enhance learning in fear conditioning. To test this idea, we introduced ChR2, or GFP, bilaterally into $Sst^{CeA\text{-}GPe}$ neurons of wild-type mice using the intersectional viral strategy, followed by optical fiber implantation in the CeA as described above (see Figure 2A, B; Figure 3A, B; Figure 4A; and Figure 5A). We subsequently trained the mice in a mild version of the fear conditioning paradigm (Figure 5B; Figure S3C), in which a weak (0.4 mA) shock was used as the US to avoid the potential ceiling effect a stronger US might have on learning.

During conditioning, three brief trains of photo-stimulation, each coinciding with a US presentation, were delivered to the CeA (Figure 5B). This manipulation increased CS^+-induced conditioned freezing behavior in the ChR2 mice compared with the GFP mice in a retrieval test 24 hours after the conditioning (Figure 5B). Interestingly, the ChR2 mice also showed an increase in freezing response to CS^- during the retrieval test (Figure 5B), albeit their discrimination index did not significantly differ from that of the GFP mice ($P = 0.19$, Welch's t-test; Figure 5C). To check if the facilitating effect on learning is because activating $Sst^{CeA\text{-}GPe}$ neurons influences valence processing, we tested these mice again in the RTPP or RTPA task for photo-stimulating $Sst^{CeA\text{-}GPe}$ neurons using the same parameters as those used in fear

conditioning. Notably, the two groups of animals behaved similarly in the test (Figure 5D, E), indicating that photo-activation of $Sst^{CeA\text{-}GPe}$ neurons is not inherently aversive or rewarding. These results together suggest that activating $Sst^{CeA\text{-}GPe}$ neurons during US presentation promotes the formation of fear memories, although the activation may not by itself produce aversive valence.

Discussion

Animals have the ability to use an environmental cue (i.e., CS) to predict the occurrence of an aversive or harmful consequence (i.e., US) – on condition that the former is frequently associated with the latter – and to show appropriate behavioral reactions based on the prediction (Lang and Davis, 2006; LeDoux, 2000; Pavlov, 1927; Schultz, 2006). Such ability is fundamental for survival and adaptation to the environment. Extensive studies, exemplified by those focusing on Pavlovian fear conditioning, have shown that the CeA plays important roles in the establishment of adaptive defensive behaviors (Duvarci and Pare, 2014; Fadok et al., 2018; Herry and Johansen, 2014; Janak and Tye, 2015; Li, 2019). However, despite the intensive study, how the CeA processes and represents the aversive US during fear conditioning, and how it contributes to the formation of aversive memories remain to be fully understood. Here, we identified a previously unknown circuit, the $Sst^{CeA\text{-}GPe}$ circuit, that is essential for fear conditioning. Specifically, we showed that Sst^{+} CeA neurons send a major projection to innervate GPe neurons, and permanent inhibition of $Sst^{CeA\text{-}GPe}$ neurons prevented fear conditioning. Moreover, $Sst^{CeA\text{-}GPe}$ neurons were excited by US but not CS during fear conditioning, and transient inactivation or activation of these neurons specifically during US presentation impaired or promoted, respectively, fear learning. One the basis of these results, we propose that the major

function of $Sst^{CeA\text{-}GPe}$ neurons in fear conditioning is to represent and process the US information, and convey this information to downstream GPe neurons, thereby instructing learning.

The GPe is a major basal ganglia structure whose roles in motor control have been the focus of investigation (Kita, 2007; Wallace et al., 2017), but whose other functions have been understudied. Nevertheless, the GPe has been implicated in regulating emotions or affects, including fear or threat. For example, human imaging studies indicate that GPe activation is associated with negative emotions, such as fear, disgust, depression and anxiety (Binelli et al., 2014; Hattingh et al., 2012; Ipser et al., 2013; Murphy et al., 2003). In addition, animal studies have shown that lesions and pharmacological or molecular manipulations in the GPe potently alter fear- or anxiety-like behaviors (Blanchard et al., 1981; Hernadi et al., 1997; Kertes et al., 2009; Sztainberg et al., 2011; Talalaenko et al., 2006). These findings thus ascribe a function of fear or threat regulation to the GPe. An obvious question is how this GPe function is related to that of the known "fear circuit", including the amygdala. A potential anatomical link between the GPe and the fear circuit is suggested by previous studies, which demonstrate the existence of the CeA to GPe projections (Hunt et al., 2018; Shinonaga et al., 1992). Nevertheless, the roles of these projections in fear regulation, and in behavior in general, have remained unknown.

Our study uncovers that these projections originate mainly from Sst^{+} CeA neurons and shows that the $Sst^{CeA\text{-}GPe}$ circuit indeed constitutes a neural substrate for fear learning. The activities of $Sst^{CeA\text{-}GPe}$ neurons may not be sufficient to cause aversive responses, as suggested by the

observation that activating these neurons produced no effect in the RTPP/RTPA test. However, the information carried by these neurons could be important for valence processing in the GPe. Future studies need to elucidate how GPe neurons interact with the upstream $Sst^{CeA\text{-}GPe}$ neurons and neurons in downstream structures to participate in fear processing and learning.

Sst^{+} CeA neurons send long-range projections to a number of target areas (Ahrens et al., 2018; Fadok et al., 2018; Li, 2019; Penzo et al., 2014; Steinberg et al., 2020; Ye and Veinante, 2019; Yu et al., 2017; Zhou et al., 2018). Some of these projections have been studied in the context of fear conditioning or anxiety-related behaviors (Ahrens et al., 2018; Penzo et al., 2014; Steinberg et al., 2020; Zhou et al., 2018). However, the encoding properties of these projections and how they contribute to specific aspects of learning or executing defensive behaviors have not been characterized. Our study pinpoints the main function of $Sst^{CeA\text{-}GPe}$ neurons being representation and processing of US information during fear conditioning. Future studies need to delineate whether and how different CeA projection pathways differentially but coordinately contribute to the establishment of defensive behaviors.

Materials and Methods

Animals

Male and female mice of 3-6 months old were used in the behavioral experiments; those of 6-10 weeks old were used in the *in vitro* electrophysiology experiments. Mice were housed under a 12-h light/dark cycle (7 a.m. to 7 p.m. light) in groups of 2-5 animals, with food and water available *ad libitum*. All behavioral experiments were performed during the light cycle.

Littermates were randomly assigned to different groups prior to experiments. All mice were bred onto a C57BL/6J background. All experimental procedures were approved by the Institutional Animal Care and Use Committee of Cold Spring Harbor Laboratory (CSHL) and performed in accordance to the US National Institutes of Health guidelines.

The C57/B6 wild-type mice were purchased from the Jackson Laboratory. The *H2B-GFP* (*Rosa26-stop^{flox}-H2B-GFP*) reporter mouse line (He et al., 2012) was generated by Z. Josh Huang's lab at CSHL. The *Sst-IRES-Cre* mice (Taniguchi et al., 2011) were purchased from the Jackson Laboratory (Stock No: 013044). The *Ai14* reporter mice (Madisen et al., 2010) were purchased from the Jackson Laboratory (Stock No: 007908).

Viral vectors and reagents

The retrograde AAV expressing Cre (AAVrg-Cre), which is suitable for retrogradely labeling CeA neurons, was newly developed and packed in Xiaoke Chen's lab at Stanford University. The AAV2/9-CAG-DIO-TeLC-eGFP was previously described (Murray et al., 2011) and custom-packed at Penn Vector Core (Philadelphia, PA, USA). The AAV9-EF1a-DIO-hChR2(H134R)-eYFP-WPRE-hGH were made by Penn Vector Core. The AAV9-CAG-Flex-GFP was produced by the University of North Carolina vector core facility (Chapel Hill, North Carolina, USA). The AAV1.Syn.Flex.GCaMP6f.WPRE.SV40, AAV1-hSyn1-SIO-stGtACR1-FusionRed and AAV2-hSyn-DIO-mCherry were produced by Addgene (Watertown, MA, USA). All viral vectors were stored in aliquots at −80°C until use.

The retrograde tracer cholera toxin subunit B (CTB) conjugated with either Alexa Fluor™ 647 or 555 (CTB-647 or CTB-555, respectively) was purchased from Invitrogen, Thermo Fisher Scientific (Waltham, Massachusetts, USA). CTB was used at a concentration of 1mg/ml in phosphate-buffered saline.

Stereotaxic Surgery

Standard surgical procedures were followed for stereotaxic injection (Li et al., 2013; Penzo et al., 2015; Yu et al., 2017; Yu et al., 2016). Briefly, mice were anesthetized with isoflurane (3% at the beginning and 1% for the rest of the surgical procedure), and positioned in a stereotaxic injection frame (myNeuroLab.com). A digital mouse brain atlas was linked to the injection frame to guide the identification and targeting (Angle Two Stereotaxic System, myNeuroLab.com). The injection was performed at the following stereotaxic coordinates for CeL: −1.22 mm from Bregma, 2.9 mm lateral from the midline, and 4.6 mm vertical from skull surface; for GPe: -0.46 mm from Bregma, 1.85 mm lateral from the midline, and 3.79 mm vertical from skull surface; and for BNST: 0.20 mm from bregma, 0.85 mm lateral from the midline, and 4.15 mm vertical from skull surface.

For virus or tracer injection, we made a small cranial window (1–2 mm^2), through which virus or fluorescent tracers (~0.3 μl) were delivered via a glass micropipette (tip diameter, ~5 μm) by pressure application (5–20 psi, 5–20 ms at 0.5 Hz) controlled by a Picrospritzer III (General Valve) and a pulse generator (Agilent). During the surgical procedure, mice were kept on a heating pad maintained at 35°C and were brought back to their home-cage for post-surgery

recovery and monitoring. Subcutaneous Metacam (1-2 mg kg–1 meloxicam; Boehringer Ingelheim Vetmedica, Inc.) was given post-operatively for analgesia and anti-inflammatory purposes. For optogenetic experiments, optical fibers (200 µm diameter, 0.22 NA, 5 mm length) were implanted bilaterally 0.3 mm over the CeA. A small metal bar, which was used to hold the mouse in the head fixation frame to connect optical fibers during training, was mounted on the skull with C&B Metabond quick adhesive cement (Parkell Inc.), followed by dental cement (Lang Dental Manufacturing Co., Inc.).

In vitro electrophysiology

For the *in vitro* electrophysiology experiments, mice were anaesthetized with isoflurane and perfused intracardially with 20 mL ice-cold artificial cerebrospinal fluid (ACSF) (118 mM NaCl, 2.5 mM KCl, 26.2 mM $NaHCO_3$, 1 mM NaH_2PO_4, 20 mM glucose, 2 mM $MgCl_2$ and 2 mM $CaCl_2$, pH 7.4, gassed with 95% O_2 and 5% CO_2). Mice were then decapitated and their brains quickly removed and submerged in ice-cold dissection buffer (110.0 mM choline chloride, 25.0 mM $NaHCO_3$, 1.25 mM NaH_2PO_4, 2.5 mM KCl, 0.5 mM $CaCl_2$, 7.0 mM $MgCl_2$, 25.0 mM glucose, 11.6 mM ascorbic acid and 3.1mM pyruvic acid, gassed with 95% O_2 and 5% CO_2). 300 µm coronal slices containing the globus pallidus externa (GPe) were cut in dissection buffer using a HM650 Vibrating-blade Microtome (Thermo Fisher Scientific). Slices were immediately transferred to a storage chamber containing ACSF at 34 °C. After 40 min recovery time, slices were transferred to room temperature (20–24°C) and perfused with gassed ACSF constantly throughout recording.

Whole-cell patch clamp recording was performed as previously described (Li et al., 2013). Briefly, recording from GPe neurons was obtained with Multiclamp 700B amplifiers and pCLAMP 10 software (Molecular Devices, Sunnyvale, California, USA), and was visually guided using an Olympus BX51 microscope equipped with both transmitted and epifluorescence light sources (Olympus Corporation, Shinjuku, Tokyo, Japan). The external solution was ACSF. The internal solution contained 115 mM cesium methanesulfonate, 20 mM CsCl, 10 mM HEPES, 2.5 mM $MgCl_2$, 4 mM Na_2ATP, 0.4 mM Na_3GTP, 10 mM sodium phosphocreatine and 0.6 mM EGTA (pH 7.2).

As the acute slices were prepared from *Sst-IRES-Cre* mice in which Sst^+ CeA neurons were infected with AAV expressing ChR2-YFP, to evoke synaptic transmission onto GPe neurons driven by $Sst^{CeA\text{-}GPe}$ neurons, a blue light was used to stimulate ChR2-expressing axons originating from $Sst^{CeA\text{-}GPe}$ neurons. The light source was a single-wavelength LED system (λ = 470 nm; http://www.coolled.com/) connected to the epifluorescence port of the Olympus BX51 microscope. A light pulse of 1 ms, triggered by a TTL signal from the Clampex software, was delivered every 10 seconds to evoke synaptic responses. Evoked inhibitory post-synaptic currents (IPSCs) were recorded at a holding potential of 0 mV and in ACSF with 100 µM AP5 and 10 µM CNQX added to block excitatory synaptic transmission. Synaptic responses were low-pass filtered at 1 kHz and were analyzed using pCLAMP 10 software. Evoked IPSCs were quantified as the mean current amplitude from 50-60 ms after stimulation.

Immunohistochemistry

For histology analysis, mice were anesthetized with Euthasol (0.2 mL; Virbac, Fort Worth, Texas, USA) and perfused transcardially with 30 mL cold phosphate buffered saline (PBS) followed by 30 mL 4% paraformaldehyde (PFA) in PBS. Brains were removed immediately from the skull and placed in PFA for at least 24 hours and then in 30% sucrose in PBS solution for 24 hours for cryoprotection. Coronal sections (50 µm) were cut using a freezing microtome (Leica SM 2010R, Leica) and placed in PBS in 12-well plates. Brain sections were first washed in PBS (3 x 5 min), incubated in PBST (0.3% Triton X-100 in PBS) for 30 min at room temperature (RT) and then washed with PBS (3 x 5 min). Next, sections were blocked in 5% normal goat serum in PBST for 30 min at RT and then incubated with the primary antibody for 12 h at 4 °C. Sections were washed with PBS (5 x 15 min) and incubated with the fluorescent secondary antibody at RT for 2 h. After washing with PBS (5 x 15 min), sections were mounted onto slides with Fluoromount-G (eBioscience, San Diego, California, USA). Images were taken using an LSM 710 laser-scanning confocal microscope (Carl Zeiss, Oberkochen, Germany).

The primary antibodies used in this study were: chicken anti-GFP (Aves Labs, catalogue number GFP1020, lot number GFP697986), rabbit anti-RFP (Rockland, catalogue number 600-401-379, lot number 34135). The fluorophore-conjugated secondary antibodies used were Alexa Fluor® 488 donkey anti-chicken IgG (H+L), Alexa Fluor® 488 goat anti-rabbit IgG (H+L) and Alexa Fluor® 555 goat anti-rabbit IgG (H+L) (Life Technologies, Carlsbad, California, USA).

Fluorescent *in situ* hybridization

Single molecule fluorescent *in situ* hybridization (smFISH) (ACDBio, RNAscope) was used to

detect the expression of *Sst* and *Prkcd* mRNAs in the central amygdala (CeA) of adult mice, which were injected in the GPe with CTB-555. 5 days after CTB injection, mice were first anesthetized under isoflurane and then decapitated. Their brain tissue was first embedded in cryomolds (Sakura Finetek, Ref 4566) filled with M-1 Embedding Matrix (Thermo Scientific, Cat. No. 1310) then quickly fresh-frozen on dry ice. The tissue was stored at -80 °C until it was sectioned with a cryostat. Cryostat-cut sections (16-µm) containing the CeA were collected and quickly stored at -80 ºC until processed. Hybridization was carried out using the RNAscope kit (ACDBio).

The day of the experiment, frozen sections were post-fixed in 4% PFA in RNA-free PBS (hereafter referred to as PBS) at RT for 15 min, then washed in PBS, dehydrated using increasing concentrations of ethanol in water (50%, once; 70%, once; 100%, twice; 5 min each). Sections were then dried at RT and incubated with Protease IV for 30 min at RT. Sections were washed in PBS three times (5 min each) at RT, then hybridized. Probes against *Sst* (Cat. No. # 404631, dilution 1:50) and *Prkcd* (Cat. No. # 441791, dilution 1:50) were applied to CeA sections. Hybridization was carried out for 2 h at 40°C. After that, sections were washed twice in PBS (2 min each) at RT, then incubated with three consecutive rounds of amplification reagents (30 min, 15 min and 30 min, at 40°C). After each amplification step, sections were washed twice in PBS (2 min each) at RT. Finally, fluorescence detection was carried out for 15 min at 40°C. The red channel was left free for detection of CTB-555 fluorescence. Sections were then washed twice in PBS, incubated with DAPI for 2 min, washed twice in PBS (2 min each), then mounted with coverslip using mounting medium. Images were acquired using an LSM780 confocal microscope equipped with 20x, 40x or 63x lenses, and visualized and processed using ImageJ and Adobe

436 Illustrator.

437

438 **Behavioral tasks**

439

440 ***Auditory fear conditioning***

441 We followed standard procedures for conventional auditory fear conditioning (Li et al., 2013;
442 Penzo et al., 2014; Penzo et al., 2015; Yu et al., 2017). Briefly, mice were initially handled and
443 habituated to a conditioning cage, which was a Mouse Test Cage (18 cm x 18 cm x 30 cm) with
444 an electrifiable floor connected to a H13-15 shock generator (Coulbourn Instruments, Whitehall,
445 PA). The Test Cage was placed inside a sound attenuated cabinet (H10-24A; Coulbourn
446 Instruments). Before each habituation and conditioning session, the Test Cage was wiped with
447 70% ethanol. The cabinet was illuminated with white light during habituation and conditioning
448 sessions.

449

450 During habituation, two 4-kHz 60-dB tones and two 12-kHz 60-dB tones, each of which was 30
451 s in duration, were delivered at variable intervals within an 8-minute session. During
452 conditioning, mice received three presentations of the 4-kHz tone (conditioned stimulus; CS^+),
453 each of which co-terminated with a 2-s 0.7-mA foot shock (unless otherwise stated), and three
454 presentations of the 12-kHz tone, which were not paired with foot shocks (CS^-). The CS^+ and
455 CS^- were interleaved pseudo-randomly, with variable intervals between 30 and 90 s within a 10-
456 minute session. The test for fear memory (retrieval) was performed 24 h following conditioning

in a novel context, where mice were exposed to two presentations of CS^+ and CS^- (>120 s inter-CS interval). The novel context was a cage with a different shape (22 cm x 22 cm x 21 cm) and floor texture compared with the conditioning cage, and was illuminated with infrared light. Prior to each use the floor and walls of the cage were wiped clean with 0.5% acetic acid to make the scent distinct from that of the conditioning cage.

For optogenetic manipulation with stGtACR1 during fear conditioning, blue light (473 nm, 5 mW; 4-s square pulse) was delivered via tethered patchcord to the implanted optical fibers. The onset of the light coincided with the onset of US (2-s 0.7 mA foot shock) presentation. For optogenetic manipulation with ChR2 during fear conditioning, blue light (473 nm, 5 mW; 30-Hz, 5-ms pulses for 2 s) was delivered via tethered patchcord to the implanted optical fibers, coinciding with the presentation of US (2-s 0.4 mA foot shock).

Animal behavior was videotaped with a monochrome CCD-camera (Panasonic WV-BP334) at 3.7 Hz and stored on a personal computer. The FreezeFrame software (Coulbourn Instruments) was used to control the delivery of both tones and foot shocks. Freezing behavior was analyzed with FreezeFrame software (Coulbourn Instruments) for the TeLC experiment. For subsequent fiber photometry and optogenetic experiments, Ethovision XT 5.1 (Noldus Information Technologies) was used to track the animal, and freezing was calculated using a custom Matlab script for improved tracking while avoiding the influence by patchcords and optic fibers attached to animal's head. Baseline freezing levels were calculated as the average freezing during the first 100 s of the session before any stimuli were presented, and freezing to the auditory stimuli was

calculated as the average freezing during the tone presentation. The average of the freezing responses to two CS^+ or CS^- presentations during recall was used as an index of fear. Discrimination Index was calculated as the difference between freezing to the CS^+ and CS^-, normalized by the sum of freezing to both tones.

Real-time place preference or aversion test

Freely moving mice were habituated to a two-sided chamber (made from Plexiglas; 23 × 33 × 25 cm for each side) for 10 min, during which baseline preference to each side was assessed. During the first test session (10 min), one side of the chamber was designated the photo-stimulation side, and mice were placed in the middle to start the experiment. Once the mouse entered the stimulation side, photo-stimulation (5-ms pulses, 30 Hz, 10 mW (measured at the tip of optic fibers)) with a 473-nm laser (OEM Laser Systems Inc., Bluffdale, Utah, USA) was turned on, and was turned off upon the mouse exiting the stimulation side. In the second test session (10 min) this procedure was repeated, with the opposite side being the stimulation side. Animal behavior was videotaped with a CCD camera (C930, Logitech) and tracked with Ethovision, which was also used to control the laser stimulation and extract behavioral parameters (position, time, distance and velocity).

***In vivo* fiber photometry and data analysis**

A commercial fiber photometry system (Neurophotometrics Ltd., San Diego, CA, USA) was used to record GCaMP6f signals in $Sst^{CeA\text{-}GPe}$ neurons *in vivo* in behaving animals through an optical fiber (200 μm fiber core diameter, 5.0 mm length, 0.37 NA; Inper, Hangzhou, China)

implanted in the CeA. A patch cord (fiber core diameter, 200 µm; Doric Lenses) was used to connect the photometry system with the implanted optical fiber. The intensity of the blue light (λ = 470 nm) for excitation was adjusted to ~20 µW at the tip of the patch cord. Emitted GCaMP6f fluorescence was bandpass filtered and focused on the sensor of a CCD camera. Photometry signals and behavioral events were aligned based on an analogue TTL signal generated by a Bpod. Mean values of signals from a region of interest were calculated and saved using Bonsai software (Bonsai), and exported to MATLAB for further analysis.

To correct for slow baseline drifting caused by photobleaching, a time-dependent baseline $F_0(t)$ was computed as described previously (Jia et al., 2011). The percentage $\Delta F/F$ was calculated as $100 \times (F(t) - F_0(t))/F_0(t)$, where $F(t)$ is the raw fluorescence signal at time t. After baseline drift correction, the fluorescence signals were z-scored relative to the mean and standard deviation of the signals in a 2 s time window immediately prior to CS onset. In this experiment, we simultaneously recorded both the calcium-dependent signals and the isosbestic signals from the GCaMP6, with the latter serving to monitor potential motion artifacts as previously described (Kim et al., 2016).

Data Analysis and Statistics

All statistics are indicated where used. Statistical analyses were performed with GraphPad Prism Software (GraphPad Software, Inc., La Jolla, CA). Normality was tested by D'Agostino-Pearson or Shapiro-Wilk normality tests. All behavioral experiments were controlled by computer systems, and data were collected and analyzed in an automated and unbiased way. Virus-injected

523 animals in which the injection site was incorrect were excluded. No other mice or data points
524 were excluded.

525

526 **Acknowledgements**

527 We thank members of the Li laboratory for helpful discussions, and Z. Josh Huang for providing
528 the *H2B-GFP* (*Rosa26-stop^{flox}-H2B-GFP*) reporter mice. This work was supported by grants
529 from EMBO (ALTF 458-2017, A.F.), Swedish Research Council (2017-00333, A.F.), Charles H.
530 Revson Senior Fellowships in Biomedical Science (A.F.), the National Institutes of Health (NIH)
531 (R01MH101214, R01MH108924, R01NS104944, B.L.), Human Frontier Science Program
532 (RGP0015/2016, B.L.), the Stanley Family Foundation (B.L.), Simons Foundation (344904,
533 B.L.), Wodecroft Foundation (B.L.), the Cold Spring Harbor Laboratory and Northwell Health
534 Affiliation (B.L.) and Feil Family Neuroscience Endowment (B.L.).

535

536 **Author contributions**

537 J.G. and B.L. conceived and designed the study. J.G. conducted the experiments and analyzed
538 data. K.Y. identified the Sst$^{CeA\text{-}GPe}$ projections and assisted with experiments. A.F. designed and
539 performed the retrograde tracing combined with smFISH experiments and analyzed data. G.T.N.
540 and X.C. developed the new AAVrg-Cre virus. R.S. assisted with the smFISH experiments. J.G.
541 and B.L. wrote the paper with inputs from all authors.

542

543 **Competing interests**

544 The authors declare that no competing interests exist.

545

546 **References**

547 Ahrens, S., Wu, M.V., Furlan, A., Hwang, G.R., Paik, R., Li, H., Penzo, M.A., Tollkuhn, J., and
548 Li, B. (2018). A Central Extended Amygdala Circuit That Modulates Anxiety. J Neurosci *38*,
549 5567-5583.

550 Baumann, B., Danos, P., Krell, D., Diekmann, S., Leschinger, A., Stauch, R., Wurthmann, C.,
551 Bernstein, H.G., and Bogerts, B. (1999). Reduced volume of limbic system-affiliated basal
552 ganglia in mood disorders: preliminary data from a postmortem study. J Neuropsychiatry Clin
553 Neurosci *11*, 71-78.

554 Binelli, C., Subira, S., Batalla, A., Muniz, A., Sugranyes, G., Crippa, J.A., Farre, M., Perez-
555 Jurado, L., and Martin-Santos, R. (2014). Common and distinct neural correlates of facial
556 emotion processing in social anxiety disorder and Williams syndrome: A systematic review and
557 voxel-based meta-analysis of functional resonance imaging studies. Neuropsychologia *64*, 205-
558 217.

559 Blanchard, D.C., Blanchard, R.J., Lee, M.C., and Williams, G. (1981). Taming in the wild
560 Norway rat following lesions in the basal ganglia. Physiol Behav *27*, 995-1000.

561 Cassell, M.D., Freedman, L.J., and Shi, C. (1999). The intrinsic organization of the central
562 extended amygdala. Annals of the New York Academy of Sciences *877*, 217-241.

563 Cassell, M.D., and Gray, T.S. (1989). The amygdala directly innervates adrenergic (C1) neurons
564 in the ventrolateral medulla in the rat. Neurosci Lett *97*, 163-168.

565 Chen, T.W., Wardill, T.J., Sun, Y., Pulver, S.R., Renninger, S.L., Baohan, A., Schreiter, E.R.,
566 Kerr, R.A., Orger, M.B., Jayaraman, V., *et al.* (2013). Ultrasensitive fluorescent proteins for
567 imaging neuronal activity. Nature *499*, 295-300.

568 Ciocchi, S., Herry, C., Grenier, F., Wolff, S.B., Letzkus, J.J., Vlachos, I., Ehrlich, I., Sprengel,
569 R., Deisseroth, K., Stadler, M.B., *et al.* (2010). Encoding of conditioned fear in central amygdala
570 inhibitory circuits. Nature *468*, 277-282.

571 Critchley, H.D., Melmed, R.N., Featherstone, E., Mathias, C.J., and Dolan, R.J. (2001). Brain
572 activity during biofeedback relaxation: a functional neuroimaging investigation. Brain *124*,
573 1003-1012.

574 Davis, M. (2000). The role of the amygdala in conditioned and unconditioned fear and anxiety.
575 in The Amygdala *ed Aggleton JP (Oxford UP, Oxford)*, 213-287.

576 Duvarci, S., and Pare, D. (2014). Amygdala microcircuits controlling learned fear. Neuron *82*,
577 966-980.

578 Duvarci, S., Popa, D., and Pare, D. (2011). Central Amygdala Activity during Fear Conditioning.
579 Journal of Neuroscience *31*, 289-294.

580 Fadok, J.P., Krabbe, S., Markovic, M., Courtin, J., Xu, C., Massi, L., Botta, P., Bylund, K.,
581 Muller, C., Kovacevic, A., *et al.* (2017). A competitive inhibitory circuit for selection of active
582 and passive fear responses. Nature *542*, 96-100.

583 Fadok, J.P., Markovic, M., Tovote, P., and Luthi, A. (2018). New perspectives on central
584 amygdala function. Curr Opin Neurobiol *49*, 141-147.

585 Garcia-Lopez, M., Abellan, A., Legaz, I., Rubenstein, J.L., Puelles, L., and Medina, L. (2008).
586 Histogenetic compartments of the mouse centromedial and extended amygdala based on gene
587 expression patterns during development. J Comp Neurol *506*, 46-74.

588 Goosens, K.A., and Maren, S. (2003). Pretraining NMDA receptor blockade in the basolateral
589 complex, but not the central nucleus, of the amygdala prevents savings of conditional fear.
590 Behav Neurosci *117*, 738-750.

591 Govorunova, E.G., Sineshchekov, O.A., Janz, R., Liu, X., and Spudich, J.L. (2015).
592 NEUROSCIENCE. Natural light-gated anion channels: A family of microbial rhodopsins for
593 advanced optogenetics. Science *349*, 647-650.

594 Hartley, N.D., Gaulden, A.D., Baldi, R., Winters, N.D., Salimando, G.J., Rosas-Vidal, L.E.,
595 Jameson, A., Winder, D.G., and Patel, S. (2019). Dynamic remodeling of a basolateral-to-central
596 amygdala glutamatergic circuit across fear states. Nat Neurosci *22*, 2000-2012.

597 Hattingh, C.J., Ipser, J., Tromp, S.A., Syal, S., Lochner, C., Brooks, S.J., and Stein, D.J. (2012).
598 Functional magnetic resonance imaging during emotion recognition in social anxiety disorder: an
599 activation likelihood meta-analysis. Front Hum Neurosci *6*, 347.

600 Haubensak, W., Kunwar, P.S., Cai, H., Ciocchi, S., Wall, N.R., Ponnusamy, R., Biag, J., Dong,
601 H.-W., Deisseroth, K., Callaway, E.M., *et al.* (2010). Genetic dissection of an amygdala
602 microcircuit that gates conditioned fear. Nature *468*, 270-276.

603 He, M., Liu, Y., Wang, X., Zhang, M.Q., Hannon, G.J., and Huang, Z.J. (2012). Cell-type-based
604 analysis of microRNA profiles in the mouse brain. Neuron *73*, 35-48.

605 Hernadi, I., Karadi, Z., Faludi, B., and Lenard, L. (1997). Disturbances of neophobia and taste-
606 aversion learning after bilateral kainate microlesions in the rat pallidum. Behav Neurosci *111*,
607 137-146.

608 Herry, C., and Johansen, J.P. (2014). Encoding of fear learning and memory in distributed
609 neuronal circuits. Nat Neurosci *17*, 1644-1654.

610 Hunt, A.J., Jr., Dasgupta, R., Rajamanickam, S., Jiang, Z., Beierlein, M., Chan, C.S., and Justice,
611 N.J. (2018). Paraventricular hypothalamic and amygdalar CRF neurons synapse in the external
612 globus pallidus. Brain Struct Funct *223*, 2685-2698.

613 Ipser, J.C., Singh, L., and Stein, D.J. (2013). Meta-analysis of functional brain imaging in
614 specific phobia. Psychiatry Clin Neurosci *67*, 311-322.

615 Janak, P.H., and Tye, K.M. (2015). From circuits to behaviour in the amygdala. Nature *517*, 284-
616 292.

617 Jia, H., Rochefort, N.L., Chen, X., and Konnerth, A. (2011). In vivo two-photon imaging of
618 sensory-evoked dendritic calcium signals in cortical neurons. Nat Protoc *6*, 28-35.

619 Kertes, E., Laszlo, K., Berta, B., and Lenard, L. (2009). Effects of substance P microinjections
620 into the globus pallidus and central nucleus of amygdala on passive avoidance learning in rats.
621 Behav Brain Res *198*, 397-403.

622 Kim, C.K., Yang, S.J., Pichamoorthy, N., Young, N.P., Kauvar, I., Jennings, J.H., Lerner, T.N.,
623 Berndt, A., Lee, S.Y., Ramakrishnan, C., *et al.* (2016). Simultaneous fast measurement of circuit
624 dynamics at multiple sites across the mammalian brain. Nat Methods *13*, 325-328.

625 Kita, H. (2007). Globus pallidus external segment. Prog Brain Res *160*, 111-133.

626 Krettek, J.E., and Price, J.L. (1978). A description of the amygdaloid complex in the rat and cat
627 with observations on intra-amygdaloid axonal connections. J Comp Neurol *178*, 255-280.

628 Lang, P.J., and Davis, M. (2006). Emotion, motivation, and the brain: reflex foundations in
629 animal and human research. Prog Brain Res *156*, 3-29.

630 LeDoux, J.E. (2000). Emotion circuits in the brain. Annu Rev Neurosci *23*, 155-184.

631 LeDoux, J.E., Iwata, J., Cicchetti, P., and Reis, D.J. (1988). Different projections of the central
632 amygdaloid nucleus mediate autonomic and behavioral correlates of conditioned fear. The
633 Journal of neuroscience : the official journal of the Society for Neuroscience *8*, 2517-2529.

634 Li, B. (2019). Central amygdala cells for learning and expressing aversive emotional memories.
635 Curr Opin Behav Sci *26*, 40-45.

636 Li, H., Penzo, M.A., Taniguchi, H., Kopec, C.D., Huang, Z.J., and Li, B. (2013). Experience-
637 dependent modification of a central amygdala fear circuit. Nature Neuroscience *16*, 332-339.

638 Madisen, L., Zwingman, T.A., Sunkin, S.M., Oh, S.W., Zariwala, H.A., Gu, H., Ng, L.L.,
639 Palmiter, R.D., Hawrylycz, M.J., Jones, A.R., *et al.* (2010). A robust and high-throughput Cre
640 reporting and characterization system for the whole mouse brain. Nature Neuroscience *13*, 133-
641 140.

642 Mahn, M., Gibor, L., Patil, P., Cohen-Kashi Malina, K., Oring, S., Printz, Y., Levy, R., Lampl,
643 I., and Yizhar, O. (2018). High-efficiency optogenetic silencing with soma-targeted anion-
644 conducting channelrhodopsins. Nat Commun *9*, 4125.

645 Murphy, F.C., Nimmo-Smith, I., and Lawrence, A.D. (2003). Functional neuroanatomy of
646 emotions: a meta-analysis. Cogn Affect Behav Neurosci *3*, 207-233.

647 Murray, A.J., Sauer, J.F., Riedel, G., McClure, C., Ansel, L., Cheyne, L., Bartos, M., Wisden,
648 W., and Wulff, P. (2011). Parvalbumin-positive CA1 interneurons are required for spatial
649 working but not for reference memory. Nat Neurosci *14*, 297-299.

650 Pavlov, I.P. (1927). Conditioned Reflexes (London: Oxford University Press).

651 Penzo, M.A., Robert, V., and Li, B. (2014). Fear conditioning potentiates synaptic transmission
652 onto long-range projection neurons in the lateral subdivision of central amygdala. The Journal of
653 neuroscience : the official journal of the Society for Neuroscience *34*, 2432-2437.

654 Penzo, M.A., Robert, V., Tucciarone, J., De Bundel, D., Wang, M., Van Aelst, L., Darvas, M.,
655 Parada, L.F., Palmiter, R.D., He, M., *et al.* (2015). The paraventricular thalamus controls a
656 central amygdala fear circuit. Nature *519*, 455-459.

657 Schultz, W. (2006). Behavioral theories and the neurophysiology of reward. Annu Rev Psychol
658 *57*, 87-115.

659 Shinonaga, Y., Takada, M., and Mizuno, N. (1992). Direct projections from the central
660 amygdaloid nucleus to the globus pallidus and substantia nigra in the cat. Neuroscience *51*, 691-
661 703.

662 Shucard, J.L., Cox, J., Shucard, D.W., Fetter, H., Chung, C., Ramasamy, D., and Violanti, J.
663 (2012). Symptoms of posttraumatic stress disorder and exposure to traumatic stressors are related
664 to brain structural volumes and behavioral measures of affective stimulus processing in police
665 officers. Psychiatry Res *204*, 25-31.

666 Steinberg, E.E., Gore, F., Heifets, B.D., Taylor, M.D., Norville, Z.C., Beier, K.T., Foldy, C.,
667 Lerner, T.N., Luo, L., Deisseroth, K., *et al.* (2020). Amygdala-Midbrain Connections Modulate
668 Appetitive and Aversive Learning. Neuron.

669 Swanson, L.W., and Petrovich, G.D. (1998). What is the amygdala? Trends Neurosci *21*, 323-
670 331.

671 Sztainberg, Y., Kuperman, Y., Justice, N., and Chen, A. (2011). An anxiolytic role for CRF
672 receptor type 1 in the globus pallidus. J Neurosci *31*, 17416-17424.

673 Talalaenko, A.N., Krivobok, G.K., Pankrat'ev, D.V., and Goncharenko, N.V. (2006).
674 Neurochemical mechanisms of the dorsal pallidum in the antiaversive effects of anxiolytics in
675 various models of anxiety. Neurosci Behav Physiol *36*, 749-754.

676 Taniguchi, H., He, M., Wu, P., Kim, S., Paik, R., Sugino, K., Kvitsiani, D., Fu, Y., Lu, J., Lin,
677 Y., *et al.* (2011). A resource of Cre driver lines for genetic targeting of GABAergic neurons in
678 cerebral cortex. Neuron *71*, 995-1013.

679 Tovote, P., Esposito, M.S., Botta, P., Chaudun, F., Fadok, J.P., Markovic, M., Wolff, S.B.,
680 Ramakrishnan, C., Fenno, L., Deisseroth, K., *et al.* (2016). Midbrain circuits for defensive
681 behaviour. Nature *534*, 206-212.

682 Veening, J.G., Swanson, L.W., and Sawchenko, P.E. (1984). The organization of projections
683 from the central nucleus of the amygdala to brainstem sites involved in central autonomic
684 regulation: a combined retrograde transport-immunohistochemical study. Brain Res *303*, 337-
685 357.

686 Wallace, M.L., Saunders, A., Huang, K.W., Philson, A.C., Goldman, M., Macosko, E.Z.,
687 McCarroll, S.A., and Sabatini, B.L. (2017). Genetically Distinct Parallel Pathways in the
688 Entopeduncular Nucleus for Limbic and Sensorimotor Output of the Basal Ganglia. Neuron *94*,
689 138-152 e135.

690 Waraczynski, M. (2016). Toward a systems-oriented approach to the role of the extended
691 amygdala in adaptive responding. Neurosci Biobehav Rev *68*, 177-194.

692 Wilensky, A.E., Schafe, G.E., Kristensen, M.P., and LeDoux, J.E. (2006). Rethinking the fear
693 circuit: the central nucleus of the amygdala is required for the acquisition, consolidation, and
694 expression of Pavlovian fear conditioning. The Journal of neuroscience : the official journal of
695 the Society for Neuroscience *26*, 12387-12396.

696 Ye, J., and Veinante, P. (2019). Cell-type specific parallel circuits in the bed nucleus of the stria
697 terminalis and the central nucleus of the amygdala of the mouse. Brain Struct Funct *224*, 1067-
698 1095.

699 Yu, K., Ahrens, S., Zhang, X., Schiff, H., Ramakrishnan, C., Fenno, L., Deisseroth, K., Zhao, F.,
700 Luo, M.H., Gong, L., *et al.* (2017). The central amygdala controls learning in the lateral
701 amygdala. Nat Neurosci *20*, 1680-1685.

702 Yu, K., Garcia da Silva, P., Albeanu, D.F., and Li, B. (2016). Central Amygdala Somatostatin
703 Neurons Gate Passive and Active Defensive Behaviors. J Neurosci *36*, 6488-6496.

704 Zhou, M., Liu, Z., Melin, M.D., Ng, Y.H., Xu, W., and Sudhof, T.C. (2018). A central amygdala
705 to zona incerta projection is required for acquisition and remote recall of conditioned fear
706 memory. Nat Neurosci *21*, 1515-1519.

707

A central amygdala-globus pallidus circuit conveys unconditioned stimulus information and controls fear learning

Jacqueline Giovanniello[1,2], Kai Yu[2 *], Alessandro Furlan[2 *], Gregory Thomas Nachtrab[3], Radhashree Sharma[2], Xiaoke Chen[3], Bo Li[1,2 #]

FIGURES AND SUPPLEMENTARY FIGURES

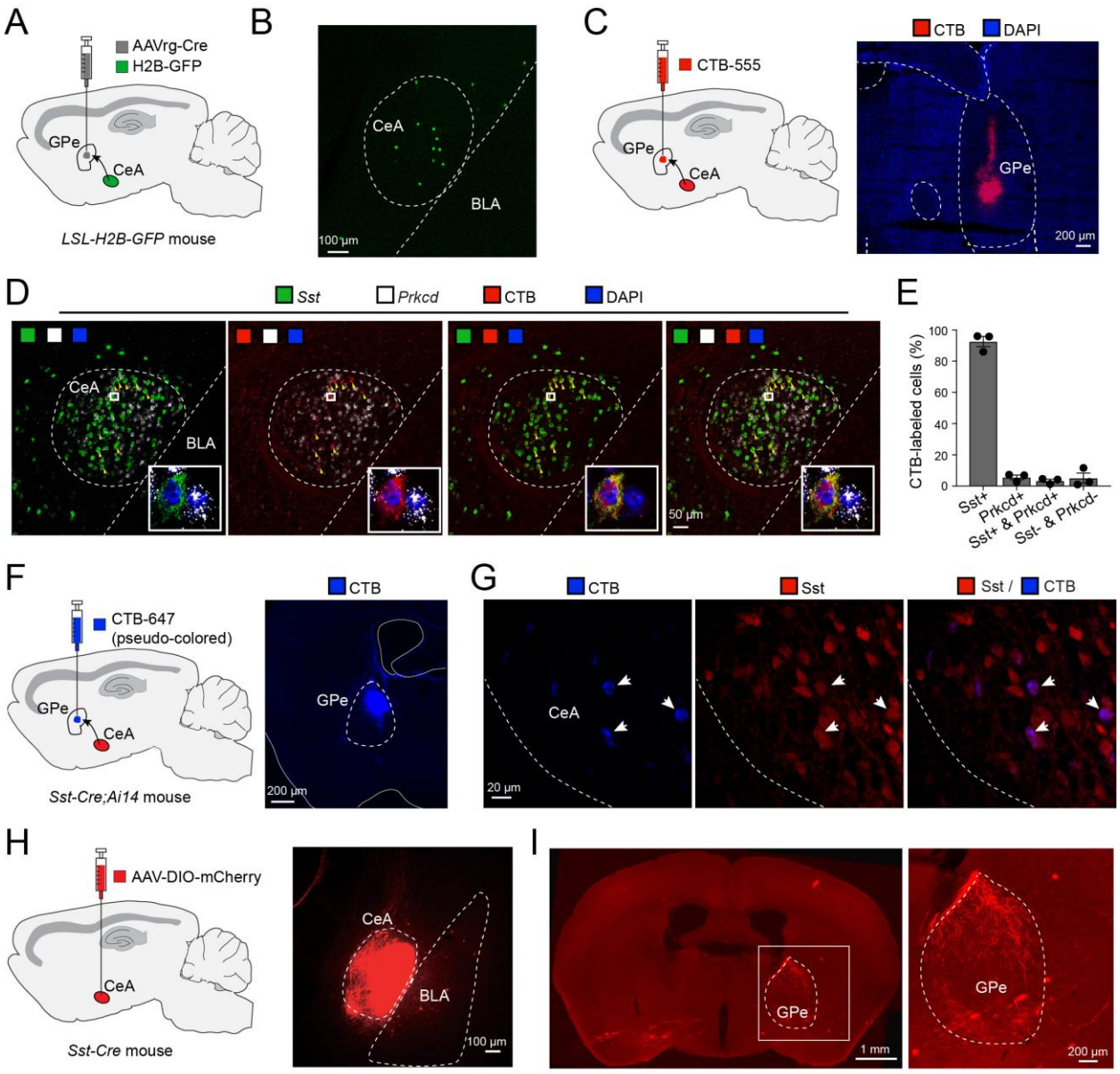

Figure 1. CeA to GPe projections originate from Sst$^+$ neurons

(A, B) A schematic of the approach (A) and a representative image showing the retrogradely-labeled H2B$^+$ cells in the CeA (B; n = 2 mice).

(C) A schematic of the approach (left) and a representative image showing the target area of CTB injection in the GPe (right).

(D) Confocal images of a coronal brain section containing the CeA from a representative mouse in which CTB was injected into the GPe (C), showing the distribution of GPe-projecting CeA neurons labeled with CTB, and the distribution of *Sst* and *Prkcd* expression detected with smFISH. Insets: high magnification images of the boxed areas in each of the images.

(E) Quantification of the percentage distribution of different types of CeA neurons that project to the GPe (data are presented as mean ± s.e.m., n = 3 mice).

(F) A schematic of the approach (left) and a representative image showing the target area of CTB injection in the GPe (right).

(G) Confocal images of a coronal brain section containing the CeA from a representative *Sst-Cre;Ai14* mouse in which CTB was injected into the GPe (F), showing the distribution of GPe-projecting CeA neurons labeled with CTB, and the distribution of Sst^+ neurons labeled with tdTomato.
(H) A schematic of the approach (left) and a representative image showing the viral infection of Sst^+ CeA neurons (red; right).
(I) Left: an image of a coronal brain section containing the GPe from a representative *Sst-Cre* mouse in which Sst^+ CeA neurons were labeled with mCherry (H). Right: a higher magnification image of the boxed area in the left, showing the distribution of axon fibers in the GPe that originate from Sst^+ CeA neurons. This experiment was repeated in 3 mice.

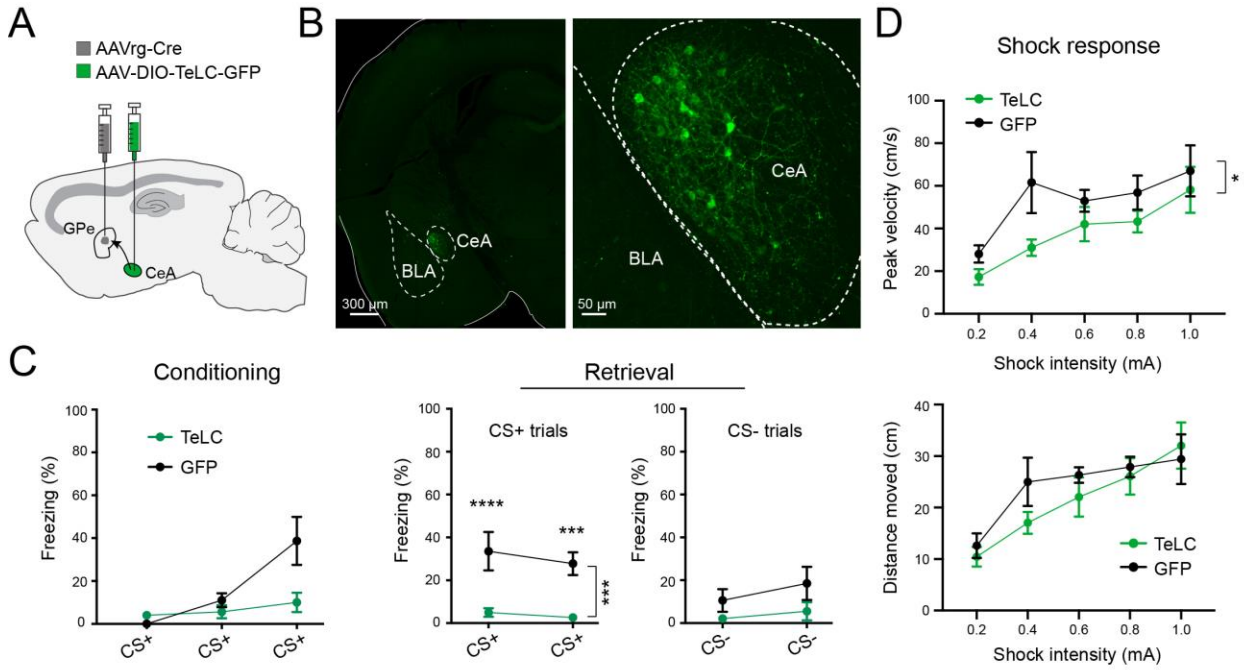

Figure 2. Inhibition of GPe-projecting CeA neurons blocks fear conditioning

(A) A schematic of the approach.

(B) Representative confocal images showing the GPe-projecting CeA neurons expressing TeLC. On the right is a higher magnification image of the amygdala area on the left.

(C) Freezing behavior in mice in which GPe-projecting CeA neurons expressed TeLC (n = 11) or GFP (n = 6), during Conditioning (left) and Retrieval (right) sessions (conditioning: $F(1,15) = 4.47$, $p = 0.052$; retrieval, CS^+ trials: $F(1,15) = 25.21$, ***$p = 0.0002$; ***$p < 0.001$, ****$p < 0.0001$; retrieval, CS^- trials: $F(1,15) = 14.41$, $p = 0.060$; two-way ANOVA with repeated measures, followed by Sidak's test).

(D) Peak velocity (top) and distance moved (bottom) for movements in mice in (C), in response to shocks of varying intensities (peak velocity: $F(1,75) = 6.359$, *$p=0.014$; distance moved: $F(1,75) = 1.619$, $p = 0.210$; two-way ANOVA).

Data in C and D are presented as mean ± s.e.m.

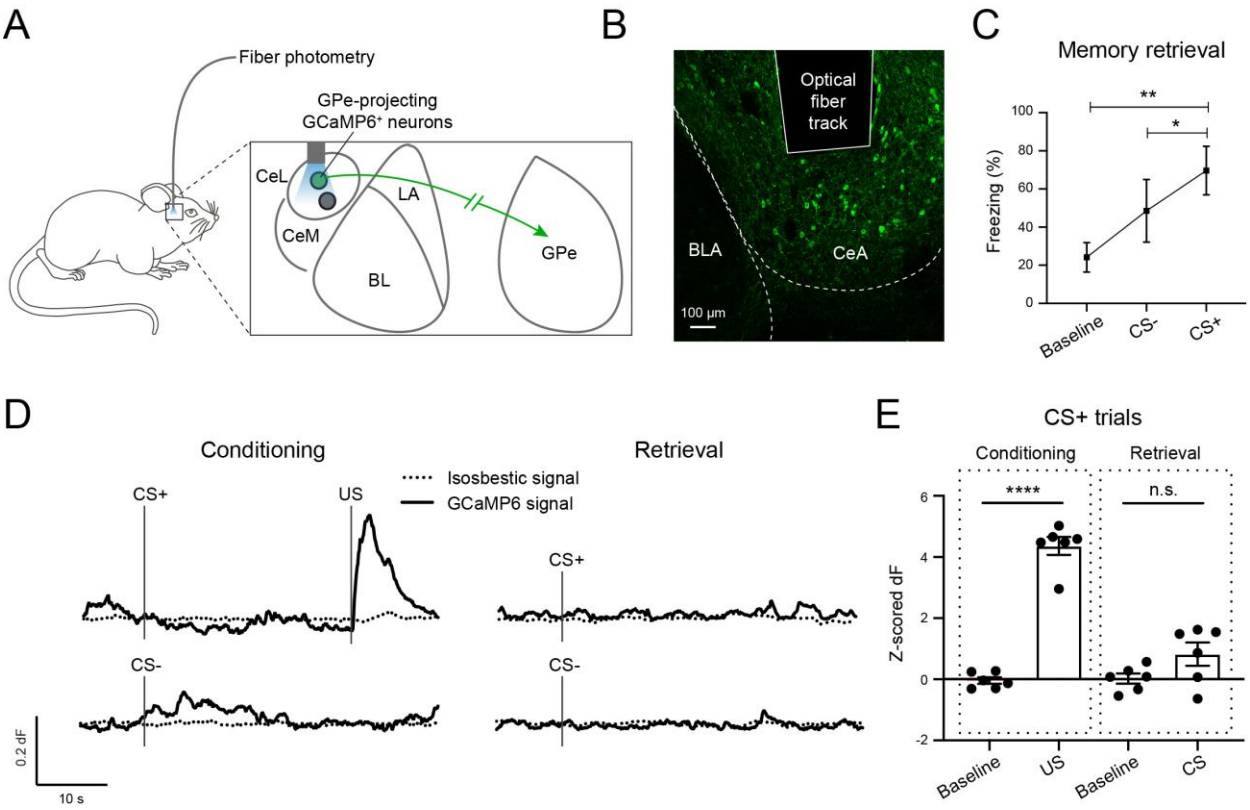

Figure 3. GPe-projecting CeA neurons encode the information about US during fear conditioning

(A) A schematic of the approach.

(B) A representative confocal image showing the GPe-projecting CeA neurons expressing GCaMP6f. The track of the implanted optic fiber is also shown.

(C) Quantification of freezing behavior during Retrieval ($F(1.314, 6.570) = 15.37$, $p=0.005$, *$p=0.023$, **$p=0.005$; one-way ANOVA followed by Tukey's test).

(D) Calcium-dependent (solid) and the simultaneously recorded isosbestic (dotted) GCaMP6 fluorescence signals in a representative mouse in CS^+ and CS^- trials for Conditioning (left), and Retrieval (right) sessions.

(E) Quantification of the calcium-dependent activities in CS^+ trials during Conditioning (left) and Retrieval (right) (n = 6 mice; $F(3,15) = 80.30$, $p<0.0001$, ****$p<0.0001$, n.s. (nonsignificant), $p>0.05$; two-way ANOVA followed by Tukey's test).

Data in C and E are presented as mean ± s.e.m.

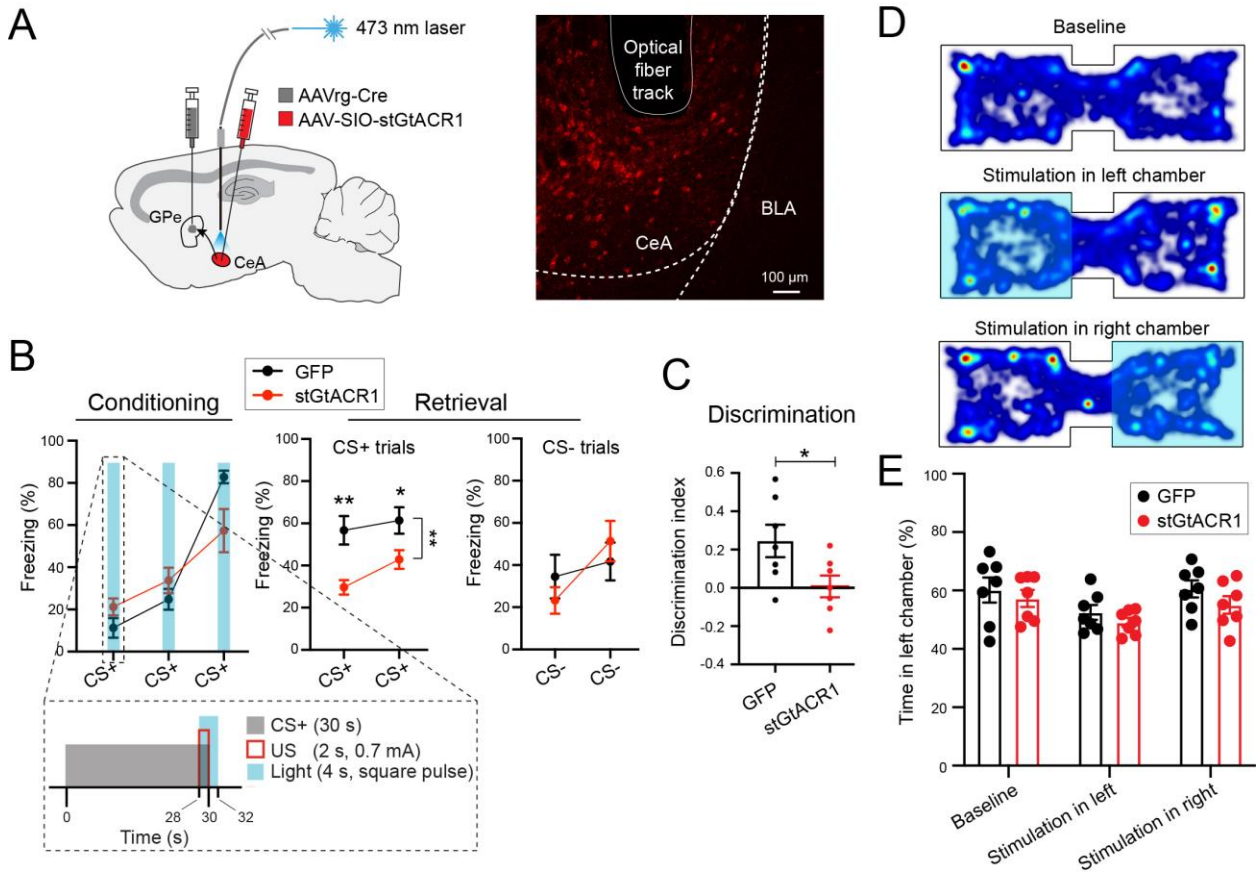

Figure 4. GPe-projecting CeA neuron activity during US presentation is necessary for learning during fear conditioning

(A) Left: a schematic of the approach. Right: a representative confocal image showing the GPe-projecting CeA neurons expressing stGtACR1. The track of the implanted optic fiber is also shown.

(B) Freezing behavior in mice in which GPe-projecting CeA neurons expressed stGtACR1 (n = 7) or GFP (n = 7), during Conditioning (left) and Retrieval (right) sessions (conditioning: $F(1,12) = 0.117$, $p > 0.05$; retrieval, CS^+ trials: $F(1,12) = 15.65$, $^{**}p = 0.002$; $^{*}p < 0.05$, $^{**}p < 0.010$; retrieval, CS^- trials: $F(1,12) = 0.010$, $p > 0.05$; two-way ANOVA with repeated measures, followed by Sidak's test). Inset shows the structure and timing of CS^+, US and light delivery.

(C) Discrimination Index calculated as $[CS^+ - CS^- / [CS^+ + CS^-]$, where CS^+ and CS^- represent the average freezing during the presentation of CS^+ and CS^-, respectively ($t(10.51) = 2.329$, $^{*}p=0.041$, Welch's t-test).

(D) Heat-maps for the activity of a representative mouse at baseline (top), or in a situation whereby entering the left (middle) or right (bottom) side of the chamber triggered photo-inactivation of GPe-projecting CeA neurons.

(E) Quantification of the mouse activity as shown in (D), for mice in which stGtaCR1 (n = 7) or GFP (n = 7) was introduced into GPe-projecting CeA neurons ($F(1, 12) = 2.135$, $p > 0.05$; two-way ANOVA with repeated measures).

Data in B, C and E are presented as mean ± s.e.m.

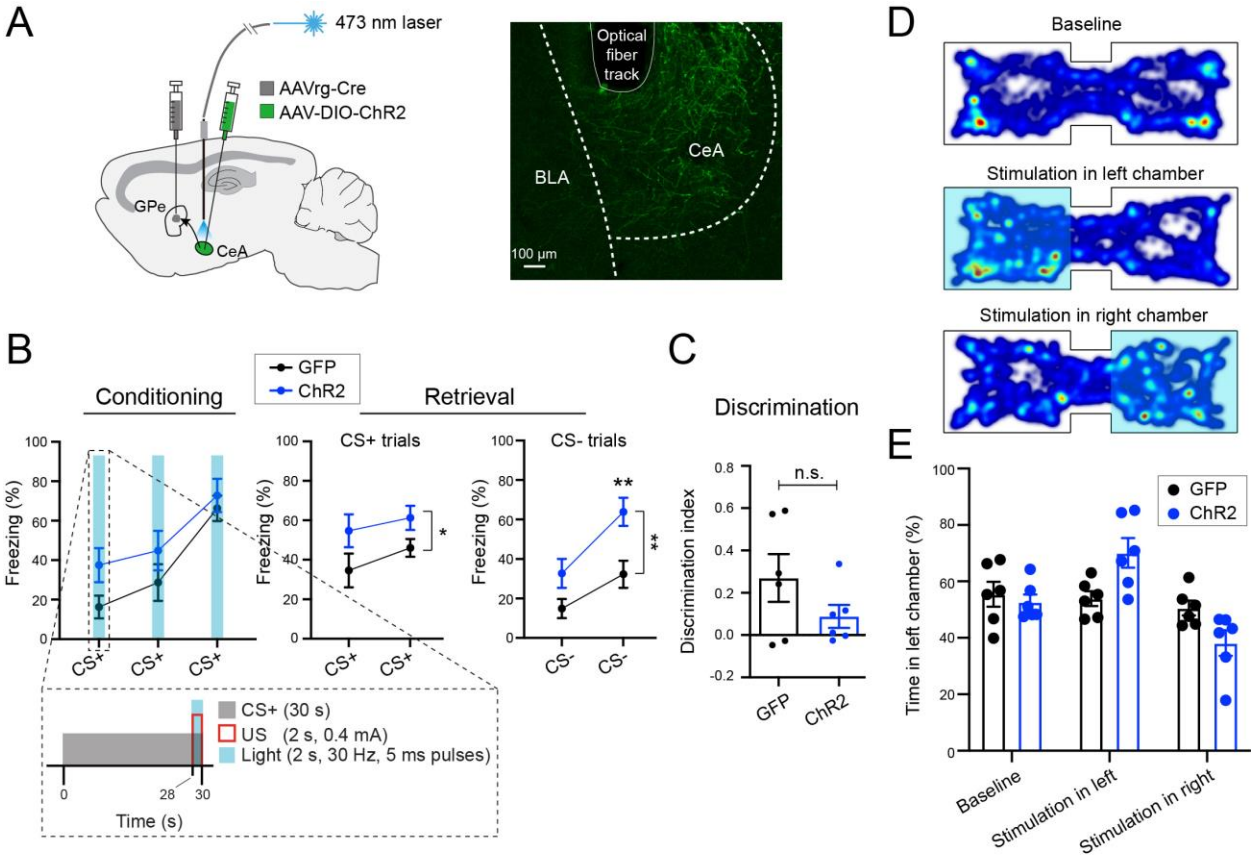

Figure 5. Activation of GPe-projecting CeA neurons during US presentation promotes fear learning

(A) Left: a schematic of the approach. Right: a representative confocal image showing the GPe-projecting CeA neurons expressing ChR2. The track of the implanted optic fiber is also shown.

(B) Freezing behavior in mice in which GPe-projecting CeA neurons expressed ChR2 (n = 6) or GFP (n = 6), during Conditioning (left) and Retrieval (right) sessions (conditioning: $F(1,10) = 3.682$, $p=0.084$; retrieval, CS^+ trials: $F(1,10) = 5.560$, $*p = 0.040$; retrieval, CS^- trials: $F(1,10) = 16.34$, $**p = 0.002$; $**p < 0.010$; two-way ANOVA with repeated measures, followed by Sidak's test). Inset shows the structure and timing of CS^+, US and light delivery.

(C) Discrimination Index calculated as $[CS^+ – CS^– / [CS^+ + CS^–]$, where CS^+ and CS^- represent the average freezing during the presentation of CS^+ and CS^-, respectively ($t(7.223) = 1.446$, $p > 0.05$, Welch's t-test).

(D) Heat-maps for the activity of a representative mouse at baseline (top), or in a situation whereby entering the left (middle) or right (bottom) side of the chamber triggered photo-activation of GPe-projecting CeA neurons.

(E) Quantification of the mouse activity as shown in (D), for mice in which ChR2 (n = 6) or GFP (n = 6) was introduced into GPe-projecting CeA neurons ($F(1,10) = 0.019$, $p > 0.05$; two-way ANOVA with repeated measures).

Data in B, C and E are presented as mean ± s.e.m.